Front. Earth Sci. 2015, 9(4): 700–708
DOI 10.1007/s11707-015-0506-7

RESEARCH ARTICLE

Internal wave parameters retrieval from space-borne SAR image

Kaiguo FAN[1,2,7], Bin FU (✉)[1], Yanzhen GU[3,6], Xingxiu YU (✉)[2,5], Tingting LIU[4], Aiqin SHI[1], Ke XU[7], Xilin GAN[1]

1 State Key Laboratory of Satellite Ocean Environment Dynamics, Second Institute of Oceanography, State Oceanic Administration, Hangzhou 310012, China
2 Faculty of Resources and Environmental Science, Hubei University, Wuhan 430062, China
3 Institute of Space and Earth Information Science, The Chinese University of Hong Kong, Hong Kong, China
4 Chinese Antarctic Center of Surveying and Mapping, Wuhan University, Wuhan 430072, China
5 Shandong Provincial Key Laboratory of Soil Conservation and Environmental Protection, Linyi University, Linyi 276000, China
6 College of Information Science and Engineering, Ocean University of China, Qingdao 266100, China
7 91039 Army, PLA, China

Abstract Based on oceanic internal wave SAR imaging mechanism and the microwave scattering imaging model for oceanic surface features, we developed a new method to extract internal wave parameters from SAR imagery. Firstly, the initial wind fields are derived from NCEP reanalysis data, the sea water density and oceanic internal wave pycnocline depth are estimated from the Levites data, the surface currents induced by the internal wave are calculated according to the KDV equation. The NRCS profile is then simulated by solving the action balance equation and using the sea surface radar backscatter model. Both the winds and internal wave pycnocline depth are adjusted by using the dichotomy method step by step to make the simulated data approach the SAR image. Then, the wind speed, pycnocline depth, the phase speed, the group velocity and the amplitude of internal wave can be retrieved from SAR imagery when a best fit between simulated signals and the SAR image appears. The method is tested on one scene SAR image near Dongsha Island, in the South China Sea, results show that the simulated oceanic internal wave NRCS profile is in good agreement with that on the SAR image with the correlation coefficient as high as 90%, and the amplitude of oceanic internal wave retrieved from the SAR imagery is comparable with the SODA data. Besides, the phase speeds retrieved from other 16 scene SAR images in the South China Sea are in good agreement with the empirical formula which describes the relations between internal wave phase speed and water depths, both the root mean square and relative error are less than 0.11 $m \cdot s^{-1}$ and 7%, respectively, indicating that SAR images are useful for internal wave parameters retrieval and the method developed in this paper is convergent and applicable.

Keywords synthetic aperture radar, internal wave, retrieval

Received July 17, 2014; accepted October 28, 2014

E-mail: binfu@sio.org.cn (Bin Fu), xxy2000@126.com (Xingxiu Yu)

1 Introduction

Oceanic internal waves are major dynamic features which travel within the interior of the ocean and play an important role in ocean mixing, acoustic signal propagation, sediment re-suspension, and cross-shore pollutant transport (Fan, 2002; Cai et al., 2003). Oceanic internal wave fields have been measured by instruments deployed in the ocean, like temperature and salinity sensors or current meters, or by acoustic instruments like sonar. However, information on internal wave fields can also be extracted from their sea surface manifestations (Zhao, 2004).

Recently, Synthetic Aperture Radar (SAR) has demonstrated the potential to obtain high-resolution ocean surface images from which internal wave features could be identified, and SAR technique for internal wave parameters retrieval has been investigated for many years (Alpers, 1985; Liu et al., 1998; Lai, 1999; Li et al., 2000; Yang et al., 2003; Fan et al., 2010).

At present, the distribution and the wavelength of internal wave could be directly extracted from SAR images (Rodenas and Garello, 1998, Alpers et al., 2005; Zheng

et al., 2007), and also the internal wave parameters, such as pycnocline depth, phase speed, group velocity and amplitude could also be retrieved from SAR images (Lai, 1999; Porter and Thompson 1999; Zhao et al., 2004; Le Caillec, 2006). This ability to provide quantitative estimates of internal wave parameters makes SAR images especially significant for ocean internal wave research.

By assuming that the local semidiurnal tide period is the generating source for these waves, and by measuring the distance between the wave packets, Li et al. (2000) calculated the group velocity of the internal waves directly from SAR images and derived both the mixed-layer depth and the amplitude under the assumption that the ocean is a two-layer finite depth model (Li et al., 2000; Yang et al., 2003). Also, Zhao et al. (2004) extracted upper layer depth and density difference from polarity conversion of internal waves observed in one RADARSAT-1 SAR image taken over the northeastern South China Sea. Porter and Thompson (1999) estimated the pycnocline depth and the density of the surface layer from the dispersion relation obtained from a two-layer fluid model.

However, the above inversion method's retrieval is constrained by the accuracy of the velocity of the internal waves, and in the case when the local semidiurnal tide period is not exactly 12.4 hours, CTD et al. data will be needed to calculate internal wave speed (Gan et al., 2007). Also, it is impossible to use the above SAR techniques to retrieve internal wave parameters from just one train of internal waves within one SAR image without the signature of polarity conversions between depression and elevation internal waves, or from one SAR image containing several trains of internal waves, but the local semidiurnal tide period is not the generating source for these waves. Besides, owing to the lack of a fully perfect microwave scattering imaging model for oceanic surface features, the above methods have not used the information of the profiles of internal waves.

Brandt et al. (1999) have studied the feasibility of retrieving ocean internal wave parameters from the internal wave profile in the SAR images based on the microwave scattering imaging model for oceanic surface features. Lai (1999) has extracted the ocean internal wave peak surface currents information through the simulated signals and the normalized radar crossing section (NRCS) from SAR images, and the peak surface currents estimates are within 15% of the observed *in situ* data. Le Caillec (2006) have also tried to estimate the pycnocline depth from profiles of the SAR signature of internal waves.

The above methods could be applied without the assumption that the local semidiurnal tide period is the generating source for these waves, but have the crucial need for the radar microwave imaging model for ocean surface. So the study of the internal wave parameters retrieval from SAR images by combining both the radar microwave imaging model and the internal waves profile NRCS in an SAR image is still in the exploratory stage.

Based on SAR imaging of internal waves, we developed a new method for internal wave parameters retrieval from space-borne SAR imagery through iteratively fitting the simulated NRCS with SAR image data. Then the wind speed, pycnocline depth, phase speed, group velocity and amplitude of the internal wave can be retrieved from SAR imagery when a best fit between simulated signals and the SAR image appears. This method is applied to several case studies in the South China Sea. The results show that the internal wave parameters, calculated from the SAR images, are in good agreement with the SODA data or the empirical formula of oceanic internal wave.

2 SAR imaging mechanism of oceanic internal wave

The SAR cannot directly observe ocean internal waves, as radar waves can penetrate seawater only a few centimeters. However, the convergent and divergent areas over the surface modulated by the oceanic internal wave will result in surface roughness variation which can be captured in the SAR image. This surface roughness variation reflects the internal wave characteristics, and therefore, we can detect the rich information about internal waves from SAR images under favorable meteorological and hydrodynamic conditions (wind conditions $2-10\,\mathrm{m\cdot s^{-1}}$) (Alpers, 1985; Thompson and Gasparovic, 1986).

Generally, imaging of oceanic internal waves by SAR can be described by hydrodynamics modulation theory, which consists of three physical processes (Alpers and Hennings, 1984; Alpers, 1985; Thompson and Gasparovic, 1986). Firstly, propagation of ocean internal waves results in the modulation of surface flow velocity. Secondly, the modulation of surface flow velocity induces the variations of the surface wave spectrum. Finally, the variation of the surface spectrum causes modulation in radar backscattering. Based on above three processes, oceanic internal wave can be imaged using SAR (Jackson and Apel, 2004).

3 SAR microwave scattering imaging ocean surface

A few imaging models for simulating radar microwave scattering from the ocean surface were developed based on the hydrodynamic theory and radar microwave scattering models, such as the Model for Fully Two-dimensional Simulation (M4S), Radar Imaging Model (RIM), Weak Hydrodynamic Interaction Theory (WHIT) and ERIM Ocean Model (EOM) (Lyzenga, 2003; Romeiser, 2005). In this paper, we use the microwave scattering imaging model for oceanic surface features of M4S developed by Dr. R. Romeiser, a software toolbox for numerical simulations of oceanic surface features with two components: wave-current interaction and radar microwave scattering (Romei-

ser et al., 1994; Romeiser and Alpers, 1997b). For the wave-current interaction, the surface wave spectra modulated by sea surface winds and surface currents are computed from the wave action balance equation by the ray tracing method (Romeiser and Alpers, 1997a). The radar microwave backscatter model is an improved composed-surface model, which can calculate the NRCS using the modulated surface wave spectra and radar parameters etc.

3.1 Wave action balance equation

The wave action balance equation describes the evolution of the energy of a wave packet traveling through a slowly varying surface current field (Alpers and Hennings, 1984) and is expressed as

$$\frac{\mathrm{d}A}{\mathrm{d}t} = \frac{\partial \Omega}{\partial k_x}\frac{\partial A}{\partial x} + \frac{\partial \Omega}{\partial k_y}\frac{\partial A}{\partial y} - \frac{\partial \Omega}{\partial x}\frac{\partial A}{\partial k_x} - \frac{\partial \Omega}{\partial y}\frac{\partial A}{\partial k_y} = S, \quad (1)$$

where $A\left(\vec{r}, \vec{k}, t\right)$ is the action spectral density of the wave packet, $\Omega\left(\vec{r}, \vec{k}, t\right)$ the apparent frequency in the moving medium, $\vec{r} = (x,y)$ the parameters of the space, $\vec{k} = (k_x,k_y)$ the wave number vectors of the wave packet, and $S\left(\vec{r}, \vec{k}, t\right)$ a source function.

In the microwave scattering imaging model, the spatially varying wave spectra were further computed by numerical integration of the wave action balance equation through the ray-tracing method.

3.2 Radar microwave backscatter model

An improved composite surface model for calculation of the ocean surface NRCS was developed in the 1990s (Romeiser et al., 1994; Romeiser and Alpers, 1997b). This kind of radar microwave backscatter model is also called a "three-scale model", because in the model, the NRCS has three components: Bragg scattering, longer-wave scattering, and short-wave scattering which is modulated by oceanic internal wave-induced surface current velocity gradients. The model can reflect the effects of surface current on the NRCS, and its results are in good agreement with the observed data (Romeiser and Alpers, 1997a). It is appropriate to use the improved composite surface model to retrieve internal wave parameters or shallow water depths from SAR images (Romeiser and Alpers, 1997a).

In the microwave scattering imaging model, radar backscattering in the presence of spatially varying surface currents induced by an oceanic internal wave is calculated by using the wave spectra from the wave action balance equation and the radar parameters.

4 Method for internal wave parameters retrieval by SAR

The evolution of nonlinear solitary internal wave trains on a continental shelf has been formulated and the wave amplitude η can be expressed by the following Korteweg-de Vries (KdV) equation (Ostrovsky and Stepanyants, 1989; Liu et a1., l998; Fan, 2002)

$$\frac{\partial \eta}{\partial t} + (C_0 + \alpha\eta + \alpha_1\eta^2)\frac{\partial \eta}{\partial x} + \beta\frac{\partial^3 \eta}{\partial x^3} + \kappa\eta - \frac{\varepsilon}{2}\frac{\partial \eta^2}{\partial x^2} = 0, \quad (2)$$

where the parameters C_0, α, α_1, β, κ and ε are the coefficients for the linear, nonlinear, high-order nonlinear, dispersion, shoaling, and dissipation effects. In a two-layer system with mixed layer depth (h_1) and bottom layer thickness (h_2), mixed layer density (ρ_1) and bottom layer density (ρ_2), the above coefficients are

$$\alpha = \frac{3C_0(h_1 - h_2)}{2h_1h_2}, \quad (3)$$

$$\beta = \frac{C_0h_1h_2}{6}, \quad (4)$$

$$C_0 = \sqrt{\frac{g\Delta\rho h_1h_2}{\rho(h_1 + h_2)}}, \quad (5)$$

where g is the gravity acceleration, ρ is the density of the water, and $\Delta\rho = \rho_2 - \rho_1$.

When the nonlinear effect is in equilibrium with the dispersion effect, the steady-state independent wave solution for Eq. (2) is

$$\eta(x,t) = \eta_0 \mathrm{sech}^2\left(\frac{x - C_pt}{l}\right), \quad (6)$$

$$U_x = \pm\left|\frac{C_0\eta_0}{h_1}\right| \mathrm{sech}^2\left(\frac{x - C_pt}{l}\right), \quad (7)$$

where η_0 is the maximum wave amplitude, C_p is the phase speed, l is the half-width of the solitary wave. U_x is the velocity of the surface current induced by the internal wave in the x direction, and the positive and negative are taken for the depression and elevation internal waves respectively. Both C_p and l are described as

$$C_p = C_0\left[1 + \frac{\eta_0(h_2 - h_1)}{2h_1h_2}\right], \quad (8)$$

$$l = \frac{2h_1h_2}{\sqrt{3\eta_0|h_2 - h_1|}}. \quad (9)$$

For the KDV equation which satisfies shallow water stereotypes of the solitary internal wave, the surface currents of internal waves will be the function of both the pycnocline depth and the amplitude of the internal wave according to Eq. (7). The amplitude could also be expressed by the pycnocline depth and the half-width of the solitary wave. Then based on the Eqs. (5), (7), (8), and (9), the formula which describes the relations between the surface currents and the pycnocline depth of the internal wave is given by,

$$U_x = \pm\left|\frac{4h_1h_2^2}{3l^2(h_2-h_1)}\sqrt{\frac{g\Delta\rho}{\rho(h_1+h_2)}}\right|\mathrm{sech}^2\left(\frac{x'}{l}\right). \quad (10)$$

Depth h can be obtained from terrain data or bathymetric survey data, and Eq. (11) will be obtained by inserting the equation $h_2 = h - h_1$ into the above equation,

$$U_x = \pm\left|\frac{4h_1(h-h_1)^2}{3l^2(h-2h_1)}\sqrt{\frac{g\Delta\rho}{\rho h}}\right|\mathrm{sech}^2\left(\frac{x'}{l}\right). \quad (11)$$

The density of the water ρ will be estimated from the Levites data, especially for ρ_1, ρ_2 and $\Delta\rho$ will also be calculated by

$$\rho_1 = \frac{1}{h_1}\int_0^{h_1}\rho(z)\mathrm{d}z, \quad (12)$$

$$\rho_2 = \frac{1}{h_2}\int_{h_1}^{h}\rho(z)\mathrm{d}z, \quad (13)$$

$$\frac{\Delta\rho}{\rho} = \frac{\rho_2-\rho_1}{(\rho_2+\rho_1)/2}. \quad (14)$$

The half-width of the solitary wave l could be directly measured by the distance D between the center of the bright band and that of the dark band in SAR imagery (Lin et al., 2010).

$$l = D/1.32. \quad (15)$$

Eq. (11) suggests that the surface currents will be determined by h_1, and then the relative NRCS ($\Delta\sigma^0$ (dB)) of internal wave SAR images is proportional to the internal wave pycnocline depth h_1, where $\Delta\sigma^0 = \sigma^0 - \sigma_0^0$, σ^0 is the ocean surface NRCS for the internal wave, σ_0^0 is the surface background NRCS.

Alpers (1985) has also shown that the relative NRCS is zero at the location of surface current velocity peaks. In other words, the backscattering is equal to the surface background NRCS (σ_0^0). So it is mainly affected by sea surface winds, and the surface wind speed could be estimated by the NRCS at the peak location (σ_M^0 (dB) or σ_0^0 (dB)) (Alpers, 1985). In our study, sea surface wind directions are derived from the National Centers for Environmental Prediction (NCEP) reanalysis data or from *in-situ* wind information.

So the inversion process starts with both initial guess parameters of h_1 and wind speeds, with radar parameters and wind direction etc. that are previously known and fixed into the microwave scattering imaging model for oceanic surface features and both wind speeds and the pycnocline depth adjusted. When all of this information is inputted into the microwave scattering imaging model for oceanic surface features, the signals induced by the internal wave can be simulated.

The appropriate initial wind speed and the pycnocline depth h_1 will speed up the convergence of simulation. In this paper, the first guessed pycnocline depth h_1 could be estimated from the Levites data and the initial wind speed is estimated by COMD-4 model (Lehner et al., 2000; Portabella and Stoffelen, 2002), where the wind direction comes from the NCEP reanalysis wind data.

During the iterative retrieval procedure, the wind speeds and the pycnocline depth are adjusted using the dichotomy method at every iteration until the best match is achieved between SAR observations and simulated data. We also define three criteria for the best match, i.e., the correlation coefficients analysis between SAR observations and the simulated signal, the difference ε analysis of σ_M^0 in SAR images and σ_{SM}^0 in simulated images, and another difference ε analysis of relative NRCS of the elongated bright and dark bands (R_{BD} (dB)) in SAR profile data and S_{BD} in the simulated profile data. Finally, the winds and the pycnocline depth h_1 could be retrieved, and are the optimum estimations.

Figure 1 gives the flow chart of internal wave parameters retrieval by SAR.

5 Results of internal wave parameters retrieval by SAR

The method for retrieving internal wave parameters from SAR images described above has been applied to one scene of SAR imagery near Dongsha Island, in the South China Sea. Figure 2 shows the ERS-2 SAR image with oceanic internal wave characteristics of elongated bright and dark features in the test site, representing the internal solitary wave packets in each train.

In order to remove the speckle noise and get the real signal of the internal wave modulation, both the Lee and mean filter with 5 × 5 filter windows (Fan et al., 2010) were used during the SAR image pre-processing. The SAR data along section A → B from the image (Fig. 2) represents the NRCS profile and the internal wave parameters would be calculated along the section A → B. The SAR image was acquired at 14:10 UTC on 23 June, 1998, the pixel size of the SAR image is about 12.5 m, and the SAR is on the ascending track with working wavelength of 5.66 cm and incidence angle of radar

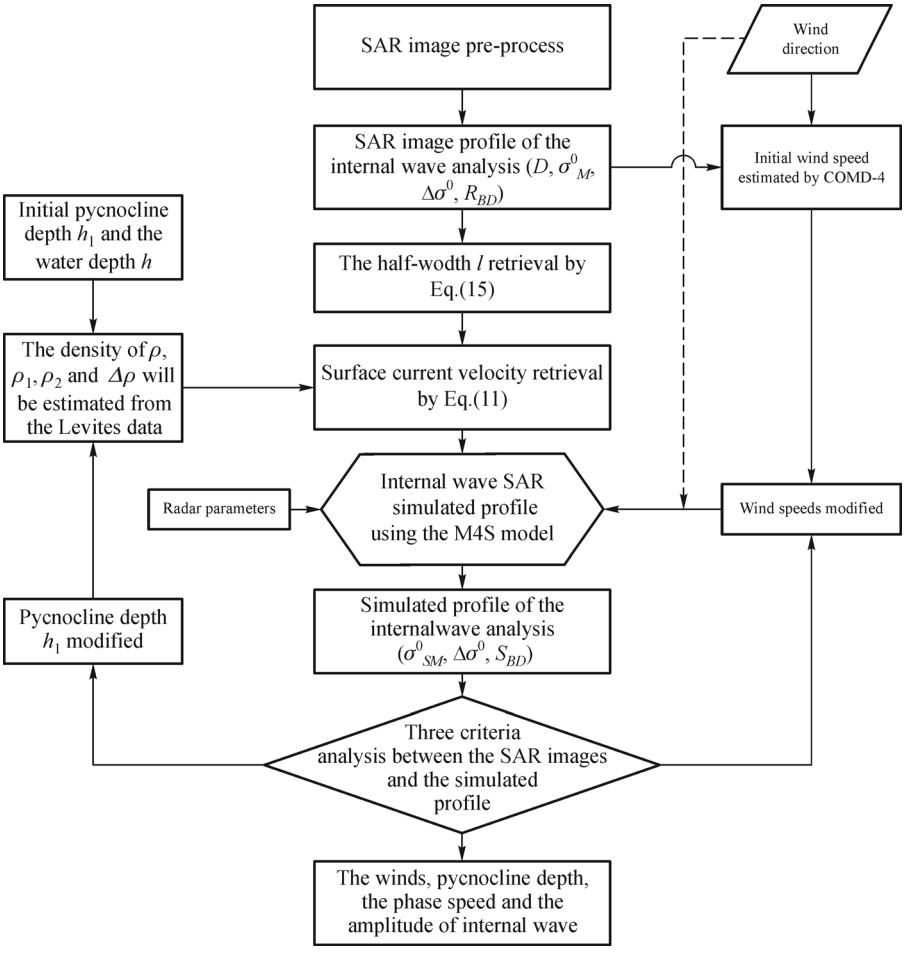

Fig. 1 The flow chart of internal wave parameters retrieval by SAR.

beam of 21.4°.

The local wind direction over the SAR imaging area is obtained from NCEP reanalysis data by Kriging interpolation, indicating south-easterlies at 12:00 UTC on June 23, 1998. During the internal wave parameters retrieval process, the initial wind speed is 2.81 $m \cdot s^{-1}$ estimated using CMOD-4 model and the pycnocline depth h_1, the density of the upper and lower layer sea water ρ_1, ρ_2, and $\Delta\rho$ estimated from the Levites data are listed in Table 1, these initial parameters can speed up the convergent rate of iteration. The water depth in the test area is 319 m based on bathymetric survey data. And the internal wave surface currents could be estimated by Eq. (11).

After several iteration steps shown on the flowchart given in Fig. 1, the final estimate of wind speed is 1.41 $m \cdot s^{-1}$, which is comparable with the wind speed obtained from NCEP reanalysis data 1.78 $m \cdot s^{-1}$, and the pycnocline depth h_1 is 97 m. Table 2 and Table 3 give the iterative process of adjusting the sea surface wind speeds and the pycnocline depth h_1. Both tables also give the difference ε analysis between σ^0_M (or σ^0_0) and σ^0_{SM}, R_{BD} and S_{BD}.

Figure 3 gives both the NRCS profile of the internal wave SAR image (the solid line), and the simulated NRCS for the internal wave (the dashed line). They have a correlation coefficient as high as 96.6%. Combining with the above difference ε analysis, these indicate that the simulated NRCS and the observations are in excellent agreement and the iterative retrieval method is convergent and applicable.

Although the amplitude has not been retrieved from the *in-situ* measurements or reanalysis data to validate the retrieved results, the amplitude of 23.9 m estimated from the SAR image is within the range of prior research reports of 20 – 50 m. Figure 4 presents the temperature and salinity profiles at 116.5°E, 21.0°N on 23 June 1998, which is in the vicinity of the internal waves observed in the SAR image, from the data of CARTON-GIESE SODA Version 2.0.2-4. These data show that the pycnocline depth h_1 is about 95 m, which suggests that the pycnocline depth h_1 calculated from the SAR image is consistent with the SODA data assimilation reanalysis.

In this paper, we also demonstrated the retrieval results from another 16 SAR images at 19 different research sites in the South China Sea. Following the iterative procedure given in Fig. 1, the internal wave parameters could be

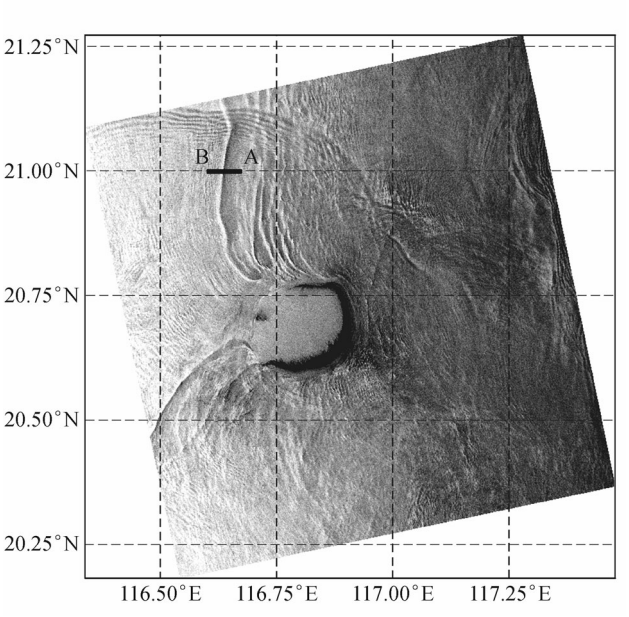

Fig. 2 ERS-2 SAR image with oceanic internal wave characteristics of elongated bright and dark features near Dongsha Island, imaging taken at 14:10 UTC on 23 June 1998, and the data line A → B represents the NRCS profile of the internal wave SAR images within the test site.

calculated from the SAR image (Table 4).

Zhang (2010) proposed an empirical formula which describes the relations between internal wave phase speed and water depths and is expressed as,

$$C_p = 0.08^* \sqrt{H}. \tag{16}$$

Table 1 Water parameters estimated from the Levites data

h_1/m	ρ_1/(kg·m^{-3})	ρ_2/(kg·m^{-3})	$\Delta\rho/\rho$
88	1,022.98	1,026.57	0.0035

Table 2 The iterative process of the adjusted sea surface wind speeds

Iterative times	Wind speeds/(m·s^{-1})	σ^0_{SM} /dB	σ^0_M /dB	Difference ε
1	2.81	−5.29	−7.46	2.17
2	2.21	−6.04	−7.46	1.42
3	1.71	−6.91	−7.46	0.55
4	1.21	−7.89	−7.46	−0.43
5	1.31	−7.61	−7.46	−0.15
6	1.41	−7.37	−7.46	0.09

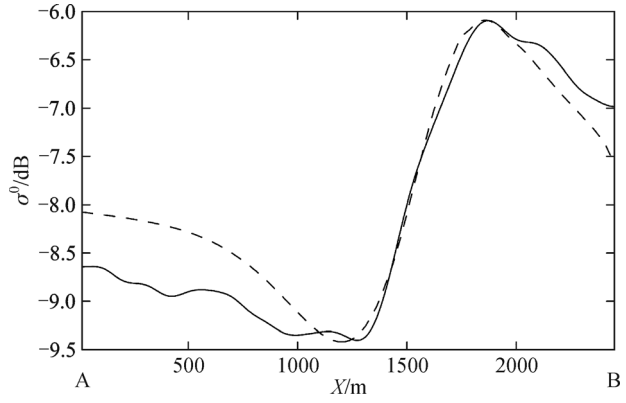

Fig. 3 The NRCS profile of the internal wave SAR image (the solid line) and the simulated signal of the internal wave (the dashed line) along the data line A → B in Fig. 2.

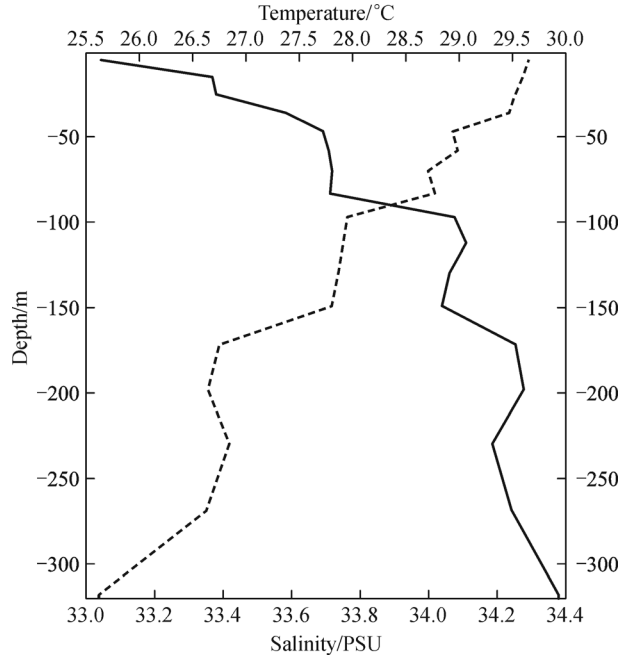

Fig. 4 Temperature and salinity profiles from CARTON-GIESE SODA data at 116.5°E, 21.0°N at the vicinity of the internal waves observed in the SAR image.

To validate the results retrieved by SAR, we compare the internal wave parameters C_p retrieved from SAR image with the phase speed calculated from the empirical formula

Table 3 The iterative process of the adjusted the pycnocline depth h_1

Iterative times	h_1/m	$\Delta\rho/\rho$	η_0/m	S_{BD}/dB	R_{BD}/dB	Difference ε
1	88	0.0035	−18.7	2.86	3.31	0.45
2	100	0.0034	−26.0	3.50	3.31	0.19
3	94	0.0034	−22.0	3.08	3.31	0.23
4	97	0.0034	−23.9	3.26	3.31	0.05

Table 4 The internal wave parameters retrieved from other SAR images

Time	Lon./(°)	Lat./(°)	Depth/m	L/m	h_1/m	η_0/m	C_p/(m·s^{-1})	C_g/(m·s^{-1})
3-12-1997	116.466	20.383	732	965.91	205	52.1	2.39	2.2
11-5-1998	116.154	20.908	378	397.73	124	64.6	1.64	1.42
23-6-1998	116.641	21.035	290	246.21	85	55.5	1.43	1.15
22-4-1998	116.414	20.581	562	653.41	162	55.3	1.98	1.78
11-5-1998	116.597	21.694	167	681.82	78	11.6	0.99	0.98
23-6-1998	116.586	21.122	283	577.65	85	9.9	1.42	1.37
23-6-1998	116.585	21.122	282	587.12	85	9.56	1.42	1.37
12-4-2000	117.321	21.749	278	331.44	107	62.9	1.33	1.18
2-10-2000	116.69	21.171	322	501.89	109	27.5	1.56	1.47
29-4-2000	115.602	21.464	109	274.62	50	17.1	0.7	0.68
28-5-2001	117.289	21.719	282	274.62	97	65.7	1.34	1.13
5-5-2001	117.091	21.459	344	568.18	100	17.1	1.44	1.37
24-4-2001	117.439	21.840	270	558.71	99	16.8	1.27	1.23
24-4-2001	117.592	21.972	134	179.92	80	29.6	0.73	0.67
24-6-2002	116.719	21.198	357	473.48	95	22.2	1.57	1.45
24-6-2002	116.775	21.351	340	464.02	85	17.2	1.47	1.37
6-11-2005	113.843	19.212	691	965.91	176	34.5	2.35	2.2
29-6-2005	116.445	21.355	307	511.36	84	12.8	1.43	1.36
29-6-2005	114.248	20.718	83	170.46	30	5.04	0.6	0.58

(Fig. 5). The error of the root mean square is 0.09 m·s^{-1} and the relative error is 6.9%, which shows that the retrieval results agree well the empirical formula.

6 Discussion and conclusions

A new method for estimating internal wave parameters, including wind speed, pycnocline depth, phase speed, group velocity and amplitude, using space-borne SAR imagery is introduced based on SAR internal wave imaging mechanism and the radar microwave scattering imaging model. The convergence and applicability of this method is tested by difference ε analysis of three criteria between the simulated NRCS profile and that from the SAR image, such as correlation coefficient etc., and also the comparison demonstrates that the internal wave parameters retrieved from SAR images are comparable with the SODA data assimilation reanalysis and are in good agreement with the empirical formula.

Taking advantage of the iterative procedure, we do not need to assume the dynamic model of the ocean internal waves when doing the retrieval. Thus, this method can be applied to any internal wave case under any stratification and any water depth. Also, since the microwave scattering imaging model is applied during the iterative process, this will reduce the speckle noise in SAR image. However, this method employs just a one dimensional model and works well only under the condition in which the pycnocline depth is not close to half of the water depth.

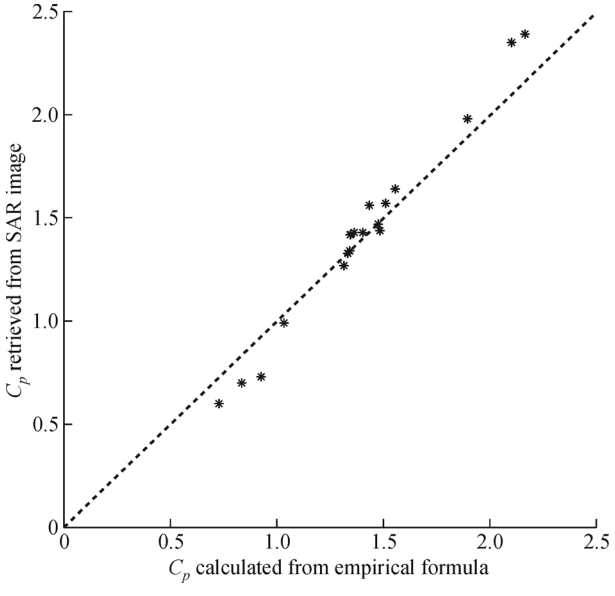

Fig. 5 Comparison between both the phase speeds retrieved from SAR image and the results calculated from the empirical formula.

Applications of the method to SAR images in the South China Sea indicate that the simulated internal wave NRCS

is consistent with the SAR data. Their correlation coefficient is as high as 90%. The pycnocline depths h_1 calculated from SAR images are consistent with the SODA data assimilation reanalysis. Also, when the phase speeds C_p retrieved from SAR images are compared with the empirical formula, the root mean square is within $0.11\ \mathrm{m\cdot s^{-1}}$ with relative errors less than 7%, indicating the method introduced in this paper is reliable and practical. There are several sources of error inherent in the difference comparison. The numerical models used in this study are not perfect and thus introduce some errors. There are also errors associated with the calculation procedure, the initial conditions, the radar microwave scattering imaging model and the SAR image quality.

Although the new method for internal wave parameters retrieval by space-borne SAR imagery introduced in this paper may not be precisely accurate, such a technique is the best way to retrieving the internal wave parameters in remote coastal areas where the internal wave group velocity could not be easily detected or where just one internal solitary wave existed. In the future, *in-situ* measurements and studies are required to address the validation of the method to overcome the limitations of the present method. These could be operated in most coastal areas day and night.

Acknowledgements We would like to thank Remote Sensing Ground Station of China, Chinese Academy of Sciences (CAS) and European Space Agency for providing the ERS-1/2 SAR, ENVISAT ASAR and Radarsat-1 SAR images, the CISL Research Data Archive (RDA) for providing the NCEP reanalysis wind data, both http://www.nodc.noaa.gov/ and http://iridl.ldeo.columbia.edu for providing the Levitus98 data and SODA data, and Dr. R. Romeiser for sharing the radar microwave backscatter imaging model of M4S. This research is jointly supported by the National Natural Science Foundation of China (Grant Nos. 41106155 and 41471227) and under the Open Fund of State Key Laboratory of Satellite Ocean Environment Dynamics (No. SOED1407). This work is also supported by General Research Fund of Hong Kong Research Grants Council (RGC) under grants CUHK 402912 and 403113. We also would like to thank the anonymous reviewers' comments to improve the original manuscript.

References

Alpers W (1985). Theory of radar imaging of internal waves. Nature, 314(6008): 245–247

Alpers W, He M X, Zeng K, Guo L F, Li X M (2005). The distribution of internal waves in the East China Sea and the Yellow Sea studied by multi-sensor satellite images. IGARSS, 2005, 0-7803-9050-4/05

Alpers W, Hennings I (1984). A theory of the imaging mechanism of underwater bottom topography by real and synthetic aperture radar. Journal of Geophysical Research, 89: 10529–10546

Brandt P, Romeiser R, Rubino A (1999). On the determination of characteristics of the interior ocean dynamics from radar signatures of internal solitary waves. Journal of Geophysical Research, 104(C12): 30039–30045

Cai S Q, Long X M, Gan Z J (2003). A method to estimate the forces exerted by internal solitons on cylindrical piles. Ocean Eng, 30(5): 673–689

Fan K G, Huang W G, Gan X L, Fu B (2010). Retrieving internal wave surface currents from SAR image. Journal of Remote Sensing, 14(1): 127–139 (in Chinese)

Fan Z S (2002). Research Fundamentals of Ocean Interior Mixing. Beijing: China Ocean Press

Gan X L, Huang W G, Yang J S, Zhou C B, Shi A Q, Jin W M (2007). A new method to extract internal wave parameters from sar imagery with Hilbert-Huang transform. J Remote Sensing, 11(1): 39–47 (in Chinese)

Jackson C R, Apel J R (2004). Synthetic aperture radar marine user's manual. Silver Spring, Natl. Environ. Satell. Data, and Inf. Serv., Nalt. Oceanic and Atmos. Admin., 245–262

Lai D Y (1999). Extraction of surface currents of solitary internal waves from synthetic aperture radar data. Proceedings of the IEEE Sixth Working Conference on Current Measurement. San Diego: IEEE

Le Caillec J M (2006). Study of the SAR signature of internal waves by nonlinear parametric autoregressive Models. IEEE Trans Geosci Rem Sens, 44(1): 148–158

Lehner S, Schulz-Stellenfleth J, Schättler B, Breit H, Horstmann J (2000). Wind and wave measurements using complex ERS-2 SAR wave mode data. IEEE Trans Geosci Rem Sens, 38(5): 2246–2257

Li X F, Clemente-Colón P, Friedman K S (2000). Estimating oceanic mixed layer depth from internal wave evolution observed from Radarsat-1 SAR. Johns Hopkins Apl Technical Digest, 2l(1): 130–135

Lin H, Fan K G, Shen H, Huang W G, He M X (2010). Review on remote sensing of oceanic internal wave by space-borne SAR. Progress in Geophys, 25(3): 1081–1091 (In Chinese)

Liu A K, Chang Y S, Hsu M K, Liang N K (1998). Evolution of nonlinear internal waves in the East and South China Seas. J Geophys Res, 103(C4): 7995–8008

Lyzenga D R (2003). Status of forward models for SAR observation of current features. The Coastal and Marine Applications of SAR Symposium, Svalbard, Norway

Ostrovsky L A, Stepanyants Y A (1989). Do internal solitions exist in the ocean? Rev Geophys, 27(3): 293–310

Portabella M, Stoffelen A (2002). Toward an optimal inversion method for synthetic aperture radar wind retrieval. J Geophys Res, 107(C8): 3086

Porter D L, Thompson D (1999). Continental shelf parameters inferred from SAR internal wave observations. J Atmos Ocean Technol, 16 (4): 475–487

Rodenas J A, Garello R (1998). Internal wave detection and location in SAR Images using wavelet transform. IEEE Trans Geosci Rem Sens, 36(5): 1494–1507

Romeiser R (2005). USER'S of M4S Manual. 1–31

Romeiser R, Alpers W (1997a). An improved composite surface model for the radar backscattering cross section of the ocean surface 2. Model response to surface roughness variations and the radar imaging of underwater bottom topography. J Geophys Res, 102 (C11): 25251–25267

Romeiser R, Alpers W (1997b). An improved composite surface model for the radar backscattering cross section of the ocean surface 1. Theory of the model and optimization/validation by scatterometer Data. J Geophys Res, 102: 25238–25250

Romeiser R, Schmidt A, Alpers W (1994). A three-scale composite surface model for the ocean wave-radar modulation transfer function, J Geophys Res, 99(C5): 9785–9801

Thompson R E, Gasparovic R F (1986). Intensity modulation in SAR image of internal waves. Nature, 320(27): 345–348

Yang J S, Huang W G, Zhou C H, Zhou C B, Hsu M K, Xiao Q M (2003). Nonlinear internal wave amplitude remote sensing from SAR image. Proc SPIE, 4892: 450–454

Zhang C (2010). Research on statistical characteristics of synthetic aperture radar ocean internal wave polarity conversion and parameters. Dissertation for Master degree. Hangzhou: Second Institute of Oceanography, State Oceanic Administration

Zhao Z X (2004). A study of nonlinear internal wave in the north eastern South China Sea. Dissertation for PhD degree. State of Delaware United States of America, The University of Delaware

Zhao Z X, Klemas V, Zheng Q, Yan X H (2004). Estimating parameters of a two-layer stratified ocean from polarity conversion of internal solitary waves observed in satellite SAR images. Remote Sens Environ, 92(2): 276–287

Zheng Q A, Susanto R D, Ho C R, Song Y T, Xu Q (2007). Statistical and dynamical analysis of generation mechanisms of solitary internal wave in the northern South China Sea. J Geophys Res, 112, C03021